Development of a 10/40 kW-class Reversible Solid Oxide Cell System at Forschungszentrum Jülich

Ro. Peters[a], W. Tiedemann[a], I. Hoven[a], R. Deja[a], N. Kruse[a], Q. Fang[a], L. Blum[a], and R. Peters[a]

[a] Institute of Energy and Climate Research (IEK-14), Forschungszentrum Jülich GmbH, 52428 Jülich, Germany

In 2018, a 5/15 kW reversible solid oxide cell system was developed and successfully operated. Based on these positive outcomes, a larger system in the power class of 10/40 kW was planned, with the well-established "Integrated Module" constituting a core element. This module consists of four 20-layer sub-stacks, two heat exchangers, and five heating plates. The basic structure was retained as per the previous system and the surrounding balance of plant components were adjusted in accordance with the higher power level. This adaptation is outlined using the example of an air heat exchanger. A possible efficiency optimization in electrolysis mode via a highly efficient steam generation process is also described and substantiated by experimental results.

Introduction

In recent years, Solid Oxide Cell (SOC) technology has significant attention (1–6). Significant successes have also been achieved in the development of reversible Solid Oxide Cell (rSOC) systems. For instance, Mougin et al. (7) presented test results of a 25-layer stack rSOC system that achieved a temperature of 700 °C at a power level of 2 kW. This operating point was reached with a 600 mA cm^{-2} current density and 78% steam utilization. It was shown that a high steam utilization is necessary in order to achieve a high level of system efficiency. Aicart et al. (8) was later able to demonstrate a system that achieved an output of 4.8 kW with a steam utilization of 95% and an operating temperature of 800 °C. Posdziech et al. (9) reported on the GrInHy project, whereby a system with an output of 143 kW was presented. This system contained 48 stacks, each of which consisted of 30 cells. With this system, based on the lower heating value (LHV), it was possible to achieve an efficiency of 48% in fuel cell mode and 84% in electrolysis mode. Peters et al. (10) presented the development of a 5/15 kW-class reversible Solid Oxide Cell (rSOC) system. The core element of the system was the "Integrated Module", which was adapted from fuel cell to rSOC operation. This module consisted of four sub-stacks, each of which featured 10 layers. The active cell area of the layer was 320 cm^2. It also contained fuel and air heat exchangers, arranged on top of and below the stacks, to bring the incoming gases to the operating temperature. In addition, three electrically-operated heating plates were utilized to heat up the system at the beginning of operation and to adjust the stack temperature during endothermic electrolysis. Other necessary components for the system operation, such as the evaporator, blowers, condenser, and control system were attached near the "Integrated Module" in a compact and suitable configuration. This system was extensively examined after its completion. A maximum direct current (DC) power of 5.3 kW_{DC} at a

current density of 0.5 A cm^{-2} and fuel utilization of 97.3% could be achieved in fuel cell mode. Under these conditions, 62.7% (LHV, DC) of electrical efficiency could be achieved. Furthermore, a maximum electrical input power of -14.3 kW_{DC} could be achieved in electrolysis mode with a current density of -0.89 A cm^{-2} at a steam conversion rate of 85%. An electrical efficiency of 70% (LHV, DC) was measured at this operating point. In the further course of the tests, switching between the operating modes was investigated and optimized. The change from fuel cell to electrolysis mode took approximately 13 minutes and was limited by steam generation; the opposite direction took less than three minutes.

In fuel cell mode, a maximum system fuel utilization of more than 99% was achieved through the use of an off-gas recirculation. Such a high utilization could be realized because the steam content was removed from the recirculated gas stream by condensation prior to being fed into the inlet of the stack. Furthermore, the system behavior during load variation was examined. With this system design, a minimum load of 0.1 A cm^{-2} in the fuel cell and -0.05 A cm^{-2} in the electrolysis mode could be demonstrated (11).

System Layout

Based on these outcomes, a new rSOC system with a power of 10 kW in fuel cell mode and 40 kW in electrolysis mode will be constructed. For this purpose, the stacks and supporting components must be adapted.

Integrated Module

Due to the modular structure of the Integrated Module, the power adjustment is easy to achieve. The design of the module is shown in Figure 1. Its overall dimensions are 399 x 224 x 973 mm^3 (length x width x height).

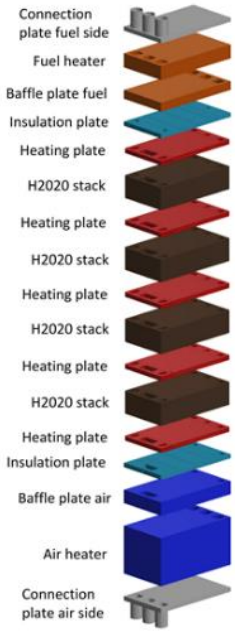

Figure 1. CAD drawing of the Integrated Module.

Four 20-layer stacks in the mark H20 design were used. The module also contained two heat exchangers, one for air (at the bottom end) and one for fuel (at the upper end). There were also five electrically-operated heating plates for the starting and cooling phases of the system and to support the endothermic electrolysis operation, as well as two insulating plates and two baffle plates. In order to connect the module to the system, two connection plates were installed at the lower and upper ends. All module components feature a plate design with a similar footprint to the stack.

System Flow Scheme

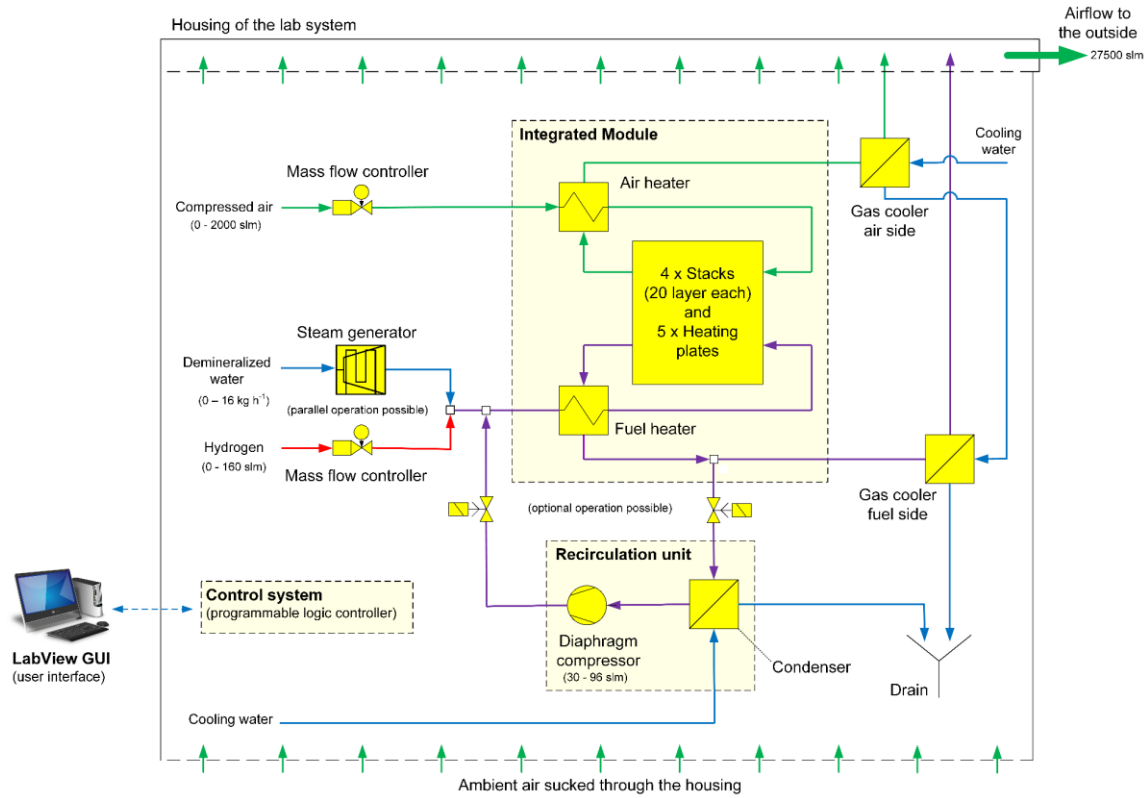

Figure 2. Flow scheme of the lab system.

The Integrated Module was subsequently inserted into a supporting system environment. The system structure is displayed schematically in Figure 2. The recirculation unit on the fuel side returns part of the exhaust exiting the module back to its inlet in order to increase the system fuel utilization in the fuel cell mode and thus its efficiency. Before entering the diaphragm compressor, the vapor content accompanying the recirculation flow was largely condensed. In electrolysis mode, the recirculation flow provided a sufficient amount of hydrogen to protect the fuel electrode material. The air was extracted from a pressurized house grid and fed into the system via a mass flow controller (MFC). The hydrogen could then be taken from a pressurized tank via an MFC and de-ionized water from a lab storage tank and transported via a pump. Then, the water was evaporated in an electrically-operated steam generator. Mixtures of any composition, consisting of steam and hydrogen, could be generated prior to combining them with the recirculation flow. After exiting the module, both exhaust gas flows were fed separately into two gas coolers and later discharged to the

outside. The system is controlled by a programmable logic controller (PLC) and all operating parameters are displayed on a graphical user interface (GUI).

Experimental Results

During development, the module components had to be adapted to the desired higher power level. To illustrate, this adaptation is shown below, using the air heat exchanger.

Air Heater

Providing the modular design of all components used in the Integrated Module, only the number of repeating units had to be adjusted compared to the 5/15 kW rSOC. One of the air heater units is shown in Figure 3. In the present case, both the fuel and air heaters feature the same plate design.

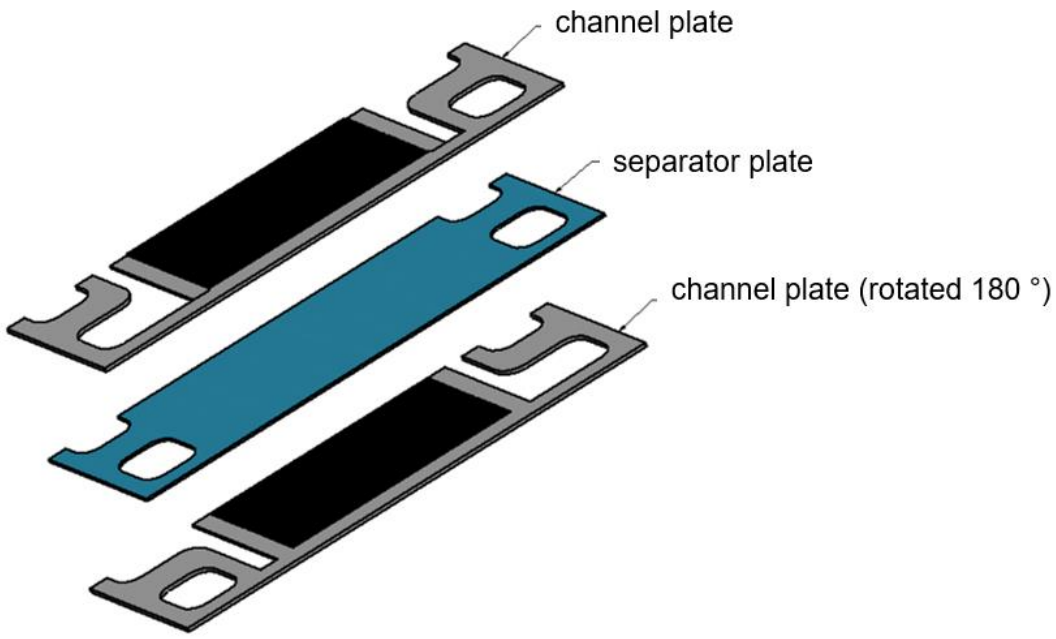

Figure 3. CAD model of the repeating unit of the air and fuel heater (half-layer width).

The repeating unit consists of two separate components, namely the channel and separator plate. All plates were designed in such a way that they can primarily be produced by means of water jet cutting and joined using a nickel-based solder in a vacuum joining process. The geometry of the flow channels is selected in such a way that a homogeneous gas distribution over the channel area, together with a low-pressure loss, can be achieved at the same time. In total, the heat exchanger consists of 13 repeating units.

After joining, the air heater was installed on a test bench, where its general performance was then tested. The location of the thermocouples in the direction of the flow is shown in Figure 4. The overall dimensions of the air heat exchanger were 399 x 224 x 217 mm^3 (length x width x height).

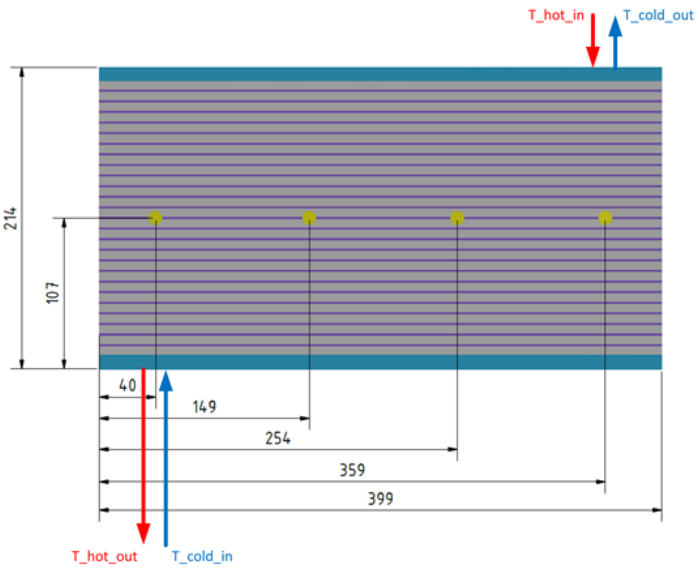

Figure 4. CAD model of the air heat exchanger with thermocouple positions. All dimensions are given in millimeters.

The tests were carried out with air as the operating medium. For the hot side, the air stream was taken from the in-house compressed air grid and later heated to the desired inlet temperature using a gas heater. Because of the existing heat losses of the supply pipeline, the inlet temperature decreased slightly when the air flow was reduced and varied between approximately 780 °C and 800 °C. On the cold side, a side channel blower sucked ambient air and downstream it was fed into the heat exchanger. Because of the increasing pressure drop with larger air flow rates, the air inlet temperature varied between 33 °C and 56 °C. During this experiment, the same amount of air was used on both sides. The results are shown in Figure 5.

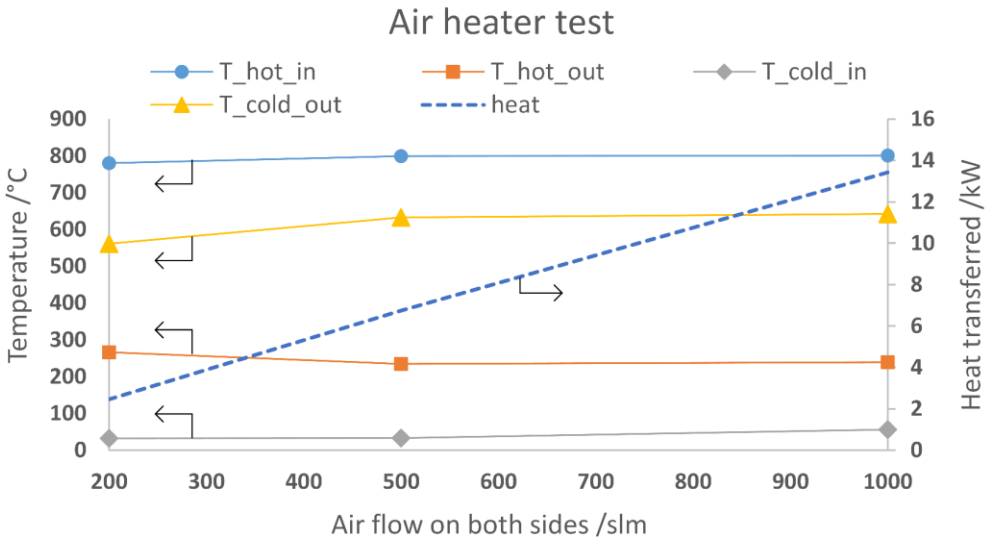

Figure 5. Experimental results of the inlet and outlet gas temperatures on both sides of the flow. The air flow rate is given in standard liters per minute (slm) based on 0 °C/1000 hPa.

The experiment reveals that the outlet temperature of the cold side remained relatively constant over a wide flow and power range, which had a positive effect on the control behavior of the system. The surface temperatures measured during the experiment are shown in Figure 6.

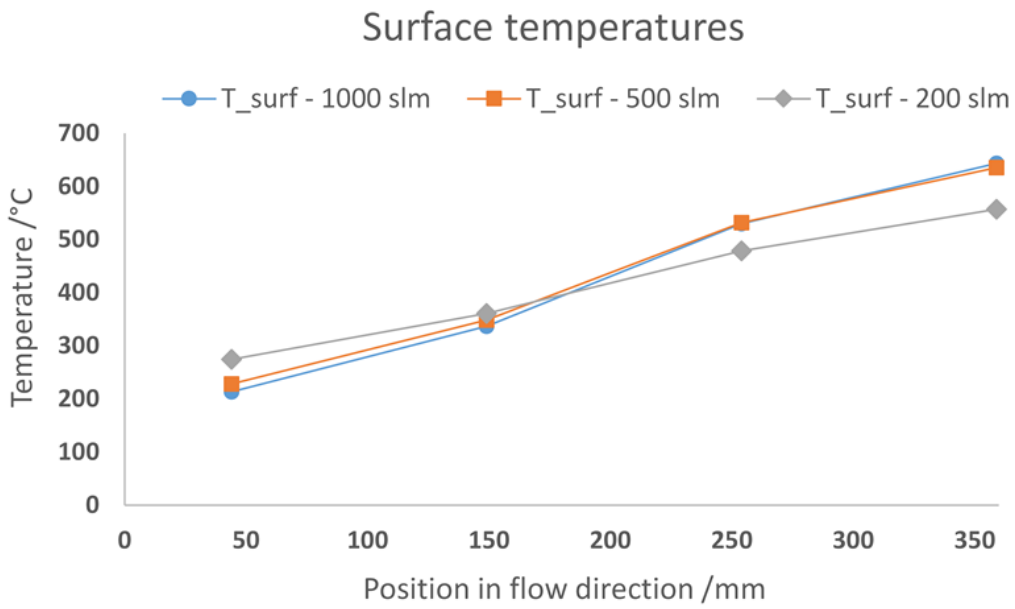

Figure 6. Experimental results of the surface temperatures (thermocouple positions according to Figure 4).

The surface temperatures also remained at a stable level between 500 and 1000 slm. Only at very low flow rates (here: 200 slm) did the slopes of the surface temperature line become somewhat flatter. This can be explained, on the one hand, by the slightly lower gas inlet temperature on the hot side and, on the other, by the different ratios of transferred heat from the hot to the cold gas sides, in combination with the heat conduction in the solid from the hot to the cold end of the air heater. With the layout properties presented here, the air heater was suitable for later use in the system. With an airflow of 1000 slm, the sum of the pressure losses on both sides were in the range of approximately 1 kPa, which has a positive effect on the power consumption of the air compressor and so also on the efficiency of the system, especially in fuel cell mode.

Steam Generator

In addition, the efficiency in electrolysis mode could be increased through a reduction of the heat losses and greater internal heat recuperation. For this reason, a steam generator with an integrated heat exchanger and an electrolysis power range of 15 kW_{el} was developed and tested. A schematic of the device design is shown in Figure 7.

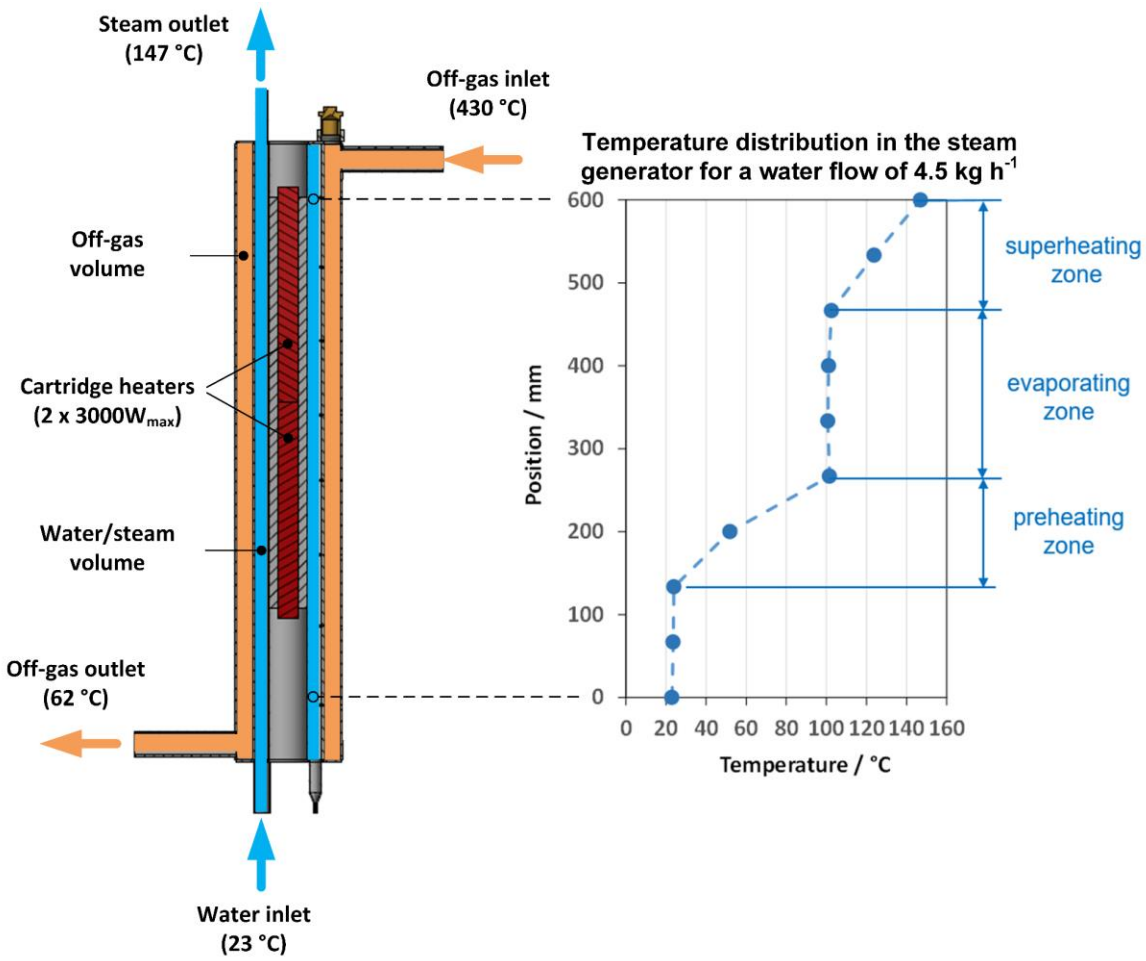

Figure 7. Schematic illustration of the steam generator (sectional view), including the associated experimental temperature distribution for a water flow of 4.5 kg h^{-1}.

This steam generator contained two heating cartridges with a maximum power of 3000 W_{el}. Both were located in the inner core of the device. The water/steam volume (blue area) was arranged cylindrically around the heating cartridges. This volume was also filled with a metallic granulate intended to help conduct the heat from the surrounding side walls into the middle of the bed and, at the same time, increase the surface area for the heat transfer to the water/steam stream. In the experiment, the inlet temperature of the water was 23 °C and a steam outlet temperature of 147 °C was reached. On the outside of the steam generator was located another cylindrical gas volume through which the fuel side off-gas (orange area) of the Integrated Module was directed in counter-flow to the water. Here, the off-gas entered the steam generator at 430 °C and left it again at 62 °C. As it flowed through, the off-gas first gives its heat to the steam and later to the steam/water mixture and cools down over the course of the process. The heat given by the off-gas reduces the electrical energy to be supplied via the heating cartridges and thereby improves the system's efficiency.

Several thermocouples were placed in the flow volume of the water/steam side at regular intervals in order to examine the course of the evaporation process. The temperature profile showed the three theoretically-expected zones in a steam generator. First, the water was heated from the inlet temperature to the evaporation temperature associated with the

pressure. As the experiment was carried out at ambient pressure, the temperature was approximately 100 °C. This section was followed by the evaporation zone, in which the temperature remained constant during the entire evaporation process. The superheating zone followed the evaporation zone, in which the temperature of the steam was increased even further. This superheating was necessary to avoid any condensation of the steam due to heat losses in the pipe and subsequent mixing with the hydrogen stream.

The positive effect on the off-gas heat recovery is investigated on the basis of the previous 5/15 kW rSOC system. With this system in full load operation, a steam utilization of 85% and a purely electrically-heated evaporator, an output of 3451 W was measured. In the steam generator test with the same media flow rates and temperatures as during system operation, an electrical input power of 2685 W was measured. This means that the electrical power supply was 766 W less than that of the steam generator used in the system. If one recalculates the system efficiency in the case of electrolysis with respect to the new steam generator, the system efficiency would increases from 70.0% to 72.8%. It can therefore be discerned that a significant increase in efficiency can be achieved via heat recovery from the off-gas streams. The high mass of this steam generator also had a disadvantageous effect. The change in the operating modes between fuel cell and electrolysis and load changes in electrolysis mode became slower and the power control of the evaporator also became more complex. For this reason, another type of steam generator is being developed in which the storage mass is lower and the output is adapted to a 10/40 kW rSOC system.

Conclusions and Outlook

An update of the Jülich Integrated Module was presented herein. With this module, all components were manufactured using plate-shaped components and, to increase performance, only the number of repeating units of the stacks or heat exchangers had to be adjusted compared to the previous system. The proven system layout was largely retained. Only the balance of plant components were adapted to the increased power range. The experimental results from the new development of the air heater and steam generator were also presented. Based on these outcomes, the new rSOC system, with a power of 10 kW in fuel cell and 40 kW in electrolysis modes, will be set up in the near future. In addition, it is intended to increase the efficiency in electrolysis mode by optimizing the system’s internal heat management. The newly developed system, as well as its test results, will then be presented at the conference for the first time.

Acknowledgments

The authors would like to thank the Helmholtz Society for financing this activity and their colleagues at the Forschungszentrum Jülich GmbH for their great support in realizing the system. In particular, we would like to thank Mr. Rabah Lekehal and Mr. Stefan Küpper for their help in setting up the lab system and Mr. Christopher Wood for his careful review of the manuscript.

References

1. M. Riedel, M.P. Heddrich and K.A. Friedrich, *J. Electrochem. Soc.*, **167**, 024504 (2020).
2. A. Hauch, R. Küngas, P. Blennow, A.B. Hansen, J.B. Hansen, B.V. Mathiesen and M.B. Mogensen, Science, **370** 186 (2020).
3. S. Megel, C. Dosch, S. Rothe, C. Folgner, N. Trofimenko, A. Rost, M. Kusnezoff, E. Reichelt, M. Jahn, A. Michaelis, C. Bienert and M. Brandner, ECS Trans., **78**(1), 3089 (2017).
4. A. Hagen and P.V. Hendriksen, ECS Trans., **78**(1), 145 (2017).
5. H. Uchida, H. Nishino, P. Puengjinda and K. Kakinuma, *J. Electrochem. Soc.*, **167**, 134516 (2020).
6. C.H. Wendel, P. Kazempoor and R.J. Braun, J. Power Sources, **276,** 133 (2014).
7. J. Mougin, S. Di Iorio, A. Chatroux, T. Donnier-Marechal, G. Palcoux, M. Petitjean and G. Roux, ECS Trans., 78 (1), 3065 (2017).
8. J. Aicart, S. Di Iorio, M. Petitjean, P. Giroud, G. Palcoux and J. Mougin, Fuel Cells, **19**(4), 381 (2019).
9. O. Posdziech, K. Schwarze and J. Brabandt, Int. J. Hydrogen Energy, **44**(35), 19089 (2018).
10. R. Peters, M. Frank, W. Tiedemann, I. Hoven, R. Deja, V.N. Nguyen, L. Blum and D. Stolten, ECS Trans., **91**(1), 2495 (2019).
11. Ro. Peters, M. Frank, W. Tiedemann, I. Hoven, R. Deja, N. Kruse, Q. Fang, L. Blum, R. Peters, *J. Electrochem. Soc.*, 168, 014508 (2021).